

Temperature and angle dependence of magnetic damping in manganite thin films

Jinghua Ren(任京华), Yuelin Zhang(张跃林), Miming Cai(蔡米铭), Yuhan Li(李语涵), Mingming Li(李明明), Tianqi Wang(王天琦), Dekun Shen(沈德坤), Hongyu Zhou(周鸿渝), Xiangwei Zhu(朱祥维), and Jinxing Zhang(张金星)
Citation: Chin. Phys. B, 2025, 34 (**10**): 107504. DOI: 10.1088/1674-1056/ade06d
http://cpb.iphy.ac.cn; http://iopscience.iop.org/cpb

What follows is a list of articles you may be interested in

Thickness-dependent magnetic property of FeNi thin film grown on flexible graphene substrate

Suixin Zhan(詹遂鑫), Shaokang Yuan(袁少康), Yuming Bai(白宇明), Fu Liu(刘福), Bohan Zhang(张博涵), Weijia Han(韩卫家), Tao Wang(王韬), Shengxiang Wang(汪胜祥), and Cai Zhou(周偲)
Chin. Phys. B, 2025, 34 (**2**): 027503. DOI: 10.1088/1674-1056/ad92fd

Low Gilbert damping in Bi/In-doped YIG thin films with giant Faraday effect

Jin Zhan(湛劲), Yi Wang(王一), Xianjie Wang(王先杰), Hanxu Zhang(张晗旭), Senyin Zhu(朱森寅), Lingli Zhang(张伶莉), Lingling Tao(陶玲玲), Yu Sui(隋郁), Wenqing He(何文卿), Caihua Wan(万蔡华), Xiufeng Han(韩秀峰), V. I. Belotelov, and Bo Song(宋波)
Chin. Phys. B, 2024, 33 (**10**): 107505. DOI: 10.1088/1674-1056/ad6b84

Spin-orbit torque effect in silicon-based sputtered Mn_3Sn film

Sha Lu(卢莎), Dequan Meng(孟德全), Adnan Khan, Ziao Wang(王子傲), Shiwei Chen(陈是位), and Shiheng Liang(梁世恒)
Chin. Phys. B, 2024, 33 (**10**): 107501. DOI: 10.1088/1674-1056/ad6079

Enhanced resonance frequency in Co_2FeAl thin film with different thicknesses grown on flexible graphene substrate

Cai Zhou(周偲), Shaokang Yuan(袁少康), Dengyu Zhu(朱登玉), Yuming Bai(白宇明), Tao Wang(王韬), Fufu Liu(刘福福), Lulu Pan(潘禄禄), Cunfang Feng(冯存芳), Bohan Zhang(张博涵), Daping He(何大平), and Shengxiang Wang(汪胜祥)
Chin. Phys. B, 2024, 33 (**3**): 037506. DOI: 10.1088/1674-1056/acfafa

Bismuth doping enhanced tunability of strain-controlled magnetic anisotropy in epitaxial $Y_3Fe_5O_{12}$(111) films

Yunpeng Jia(贾云鹏), Zhengguo Liang(梁正国), Haolin Pan(潘昊霖), Qing Wang(王庆), Qiming Lv(吕崎鸣), Yifei Yan(严轶非), Feng Jin(金锋), Dazhi Hou(侯达之), Lingfei Wang(王凌飞), and Wenbin Wu(吴文彬)
Chin. Phys. B, 2023, 32 (**2**): 027501. DOI: 10.1088/1674-1056/ac67cc

---

SPECIAL TOPIC — Advanced magnonics

Temperature and angle dependence of magnetic damping in manganite thin films

Jinghua Ren(任京华)[1,2,†], Yuelin Zhang(张跃林)[1,2,†,‡], Miming Cai(蔡米铭)[1,2,†], Yuhan Li(李语涵)[1,2], Mingming Li(李明明)[3], Tianqi Wang(王天琦)[1,2], Dekun Shen(沈德坤)[1,2], Hongyu Zhou(周鸿渝)[1,2], Xiangwei Zhu(朱祥维)[4], and Jinxing Zhang(张金星)[1,2,§]

[1] *School of Physics and Astronomy, Beijing Normal University, Beijing* 100875, *China*
[2] *Key Laboratory of Multiscale Spin Physics, Ministry of Education, Beijing* 10087, *China*
[3] *School of Physics and Microelectronics, Zhengzhou University, Zhengzhou* 450052, *China*
[4] *School of Electronics and Communication Engineering, Sun Yat-Sen University, Shenzhen* 518107, *China*

(Received 31 March 2025; revised manuscript received 13 May 2025; accepted manuscript online 4 June 2025)

Magnonics and magnonic materials have attracted widespread interest in the spintronics community and demonstrate potential for applications in the next generation of information technology. Recent advances in manganite thin films highlight their promise for magnonics, in which enhanced film quality and strain control of spin and electronic structures play a crucial role in reducing magnetic damping. Here, we report the fabrication of $La_{0.67}Sr_{0.33}MnO_3$ thin films of varying quality via pulsed laser deposition. The quality of epitaxial films is characterized using atomic force microscopy and x-ray diffraction. A pronounced fourfold anisotropy in the magnetic damping (with a ratio of about 150%) is observed, where the minimum damping occurs along the [110] crystalline orientation. Notably, improved sample quality significantly reduces the magnetic damping at low temperatures. The highest-quality sample, featuring atomic-scale terraces, exhibits a magnetic damping of $\sim 2.5 \times 10^{-3}$ at 5 K. Our results not only demonstrate effective reduction of low-temperature magnetic damping in high-quality correlated oxide systems but also provides a strategy and material platform for exploring novel quantum phenomena and for designing low-temperature magnonic devices.

Keywords: ferromagnetic resonance, correlated manganite thin film, magnetic damping

PACS: 75.30.Ds, 76.50.+g, 31.15.aq

DOI: 10.1088/1674-1056/ade06d **CSTR:** 32038.14.CPB.ade06d

1. Introduction

Spin waves can propagate over long distances within low-damping magnetic materials without involving electron motion, resulting in minimal heat dissipation. This advantage positions spin waves as promising candidates for next-generation information technology.[1] Consequently, research on magnonic material systems has advanced significantly.[2–4] The perovskite manganite, as a strongly correlated electron system, has attracted extensive attention in spintronics[5] and magnonics[6] due to its unique physical properties and tunability, such as remarkable colossal magnetoresistance,[7] metal–insulator transition[8,9] and nontrivial spin textures.[10,11] Among these, $La_{0.67}Sr_{0.33}MnO_3$ (LSMO) with the doping ratio of 0.33 for Sr exhibits not only an above-room-temperature Curie temperature ($\sim$ 370 K) with excellent ferromagnetic properties but also a half-metallic nature with low residual resistivity ($\leq 10^{-4}$ Ω·cm). The near-complete spin polarization ($\sim$ 100%) of LSMO was reported in spin-polarized photoemission[12] and tunnel magnetoresistance[13] experiments, which establishes a fundamental basis for its applications in spintronic devices.

Recently, numerous breakthroughs in magnonics have been reported in strained LSMO thin films, including magnetization modulation induced by twinned structural order and magnonic crystals in LSMO/$SrTiO_3$ films,[14] low-density current control of spin wave propagation in LSMO/$LaAlO_3$ films,[15] anisotropic spin-wave propagation,[16] coexisting nonreciprocities of spin-wave propagation originated from strain-driven Dzyaloshinskii–Moriya interaction and the stabilization of topological magnetic skyrmions at room temperature,[11] nonlinear three-magnon scattering between magnon energy bands,[17] and long-distance propagation of chiral magnonic edge states in quasi-antiferromagnetic spin textures.[18] These results provide critical experimental foundations for constructing low-power magnonic integrated circuits.

The functionality of LSMO has been further enhanced by constructing heterostructures with interface engineering or strain modulation. In multiferroic het-

[†]These authors contributed equally to this work.
[‡]Corresponding author. E-mail: yuelin.zhang@bnu.edu.cn
[§]Corresponding author. E-mail: jxzhang@bnu.edu.cn

© 2025 Chinese Physical Society and IOP Publishing Ltd. All rights, including for text and data mining, AI training, and similar technologies, are reserved.

erostructures containing ferromagnetic LSMO and ferroelectric $BiFeO_3$ or $BaTiO_3$, magnon–phonon coupling and the long-range propagation of coherent magnon-polaritons have been experimentally observed.[19–21] Spin pumping and interfacial spin transport have been studied in heterostructures containing materials with strong spin–orbit coupling, such as Pt[22,23] and $SrRuO_3$.[24] Interestingly, the extremely long-range Josephson coupling has been demonstrated in LSMO/$YBa_2Cu_3O_7$ ferromagnet–superconductor heterostructures.[25] These achievements highlight the immense potential of LSMO heterostructures in spintronic and magnonic devices based on magnetoelectric effects and superconductivity.[26] The discovery of the above phenomena has imposed very high requirements on the quality of LSMO films, specifically, the relationship between sample quality and low-temperature damping remains to be systematically studied.

Here, we report the epitaxial growth of LSMO films with a thickness of $\sim$ 120 nm on (110)-oriented $NdGaO_3$ (NGO) single-crystal substrates. A remarkable fourfold symmetric anisotropy in the magnetic damping constant is observed in these LSMO/NGO (110) films. Notably, while the room-temperature magnetic damping of all samples falls within a similar range, the highest-quality sample exhibits a significantly lower damping constant of 2.5×10^{-3} at 5 K, which is attributed to the suppression of intraband scattering by improving sample quality.

2. Experimental methods

Single-crystalline epitaxial thin films with high quality are crucial for probing the fundamental properties and mechanisms of phenomena, thereby providing a robust material platform for novel spintronic and magnonic devices. Therefore, we prepared epitaxial LSMO/NGO films, as schematically illustrated in Fig. 1(a). LSMO thin films with a thickness of $\sim$120 nm were grown on NGO (110) substrates by pulsed laser deposition using an excimer laser (248 nm). The substrates were heated to 820 °C, and the films were deposited under an oxygen atmosphere of 23 Pa using a pulsed laser with an energy density of $\sim$ 0.65 J/cm^2 at 5 Hz for 30 minutes. After deposition, the samples were cooled at a rate of 5 °C/min under an oxygen atmosphere of 10^4 Pa. The crystal structure of sample A was analyzed by x-ray θ–2θ diffraction (XRD) using Cu $K\alpha$ radiation ($\lambda = 0.15406$ nm), as shown in Fig. 1(b), which confirms the high-quality single-crystal epitaxy. Bulk LSMO crystallizes in a trigonal structure with a tilted pseudo-cubic unit cell, $a_{\text{bulk}} = b_{\text{bulk}} = c_{\text{bulk}} = 3.894$ Å.[27] The NGO (110) substrate has an orthorhombic crystal structure with a monoclinic pseudo-cubic lattice, $a_{\text{bulk}} = b_{\text{bulk}} = c_{\text{bulk}} = 3.864$ Å. Therefore, the substrate provides in-plane compressive and out-of-plane tensile strains to the LSMO film. The XRD pattern shows the $2\theta = 46.42°$ peak associated with the (002) plane of the LSMO pseudo-cubic phase. The out-of-plane lattice constant $c = 3.92$ Å was calculated using Bragg's law.

The basic magnetic properties of LSMO films were characterized by a vibrating sample magnetometer (VSM). The Curie temperature of sample A was determined to be 371 K by temperature-dependent magnetic moment measurement, as shown in Fig. 1(c). It should be noted that the magnetization of LSMO on the NGO substrate is slightly larger than that on other substrates due to the contribution of the paramagnetic NGO substrate.[28] The in-plane easy axis shows a saturated field of $\sim$ 40 mT and a coercive field of $\sim$ 3 mT along the $[010]_{\text{pc}}$ orientation, with a saturation magnetization of $\sim$ 440 emu/cc, as shown in Fig. 1(d). The out-of-plane magnetic hysteresis loop shows a saturated field of $\sim$ 420 mT and a coercive field of $\sim$ 2.9 mT along the $[001]_{\text{pc}}$ orientation. Previous studies have demonstrated that the distinct lattice constant difference between the *a*- and *b*-axes in the NGO substrate induces a uniaxial in-plane compressive strain in the epitaxial LSMO film, which generates a strongly negative perpendicular magnetic anisotropy and a slight in-plane magnetic anisotropy.[11,27]

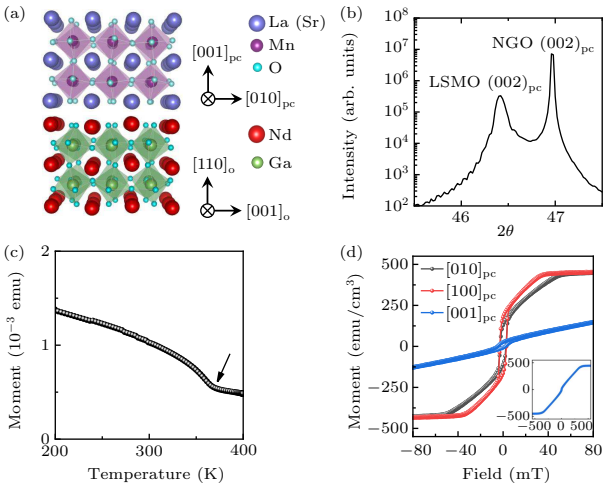


Fig. 1. Structural and magnetic characterizations of LSMO thin films at room temperature. (a) Schematic diagram of the crystal structure of the LSMO film on the NGO (110) substrate, where the subscript pc (o) represents pseudo-cubic (orthorhombic) phase. (b) The x-ray θ–2θ diffraction around the $(002)_{\text{pc}}$ peak of sample A. (c) Magnetic moment as a function of temperature of sample A. The black arrow points out the Curie temperature of about 371 K. (d) The magnetic hysteresis loop of sample A. The inset shows the complete out-of-plane hysteresis loop.

The magnetic damping of LSMO thin films was experimentally determined through ferromagnetic resonance (FMR) spectroscopy. The experiments were performed in a commercial physical property measurement system (PPMS) equipped with a superconducting magnet, providing precise control of the applied magnetic field in the in-plane geometry. A high-frequency microwave source was utilized to excite magnetization dynamics through a custom-built broadband coplanar

waveguide, while the detection of the resonance signals was achieved using a lock-in amplifier with a diode detector. The in-plane external magnetic field was applied perpendicular to the excitation field from the waveguide.

3. Experimental results

The dynamic magnetic responses of LSMO thin films at room temperature are presented in Fig. 2. The power derivative absorption spectra for a series of fixed excited frequencies f (from 3 GHz to 19 GHz) are displayed in Fig. 2(a), with the sweeping external in-plane magnetic fields applied along the $[010]_{pc}$ orientation. Figures 2(b) and 2(c) show the corresponding frequency dependence of the resonance field and the peak-to-peak linewidth (ΔH_{pp}), respectively. The relationship between the resonance field H_{ext} and the resonance frequency f follows the Kittel mode[29]

$$f = \frac{\gamma\mu_0}{2\pi}\sqrt{(H_r + H_{ani})(H_r + H_{ani} + M_s)}, \tag{1}$$

where $\gamma/(2\pi) = 28$ GHz/T is the gyromagnetic ratio, which is estimated from the FMR experimental results. M_s is the saturated magnetization, H_r is the resonance field, and H_{ani} is the anisotropy field. The magnetic damping parameter of LSMO thin films is determined by fitting the frequency dependence of the peak-to-peak linewidths ΔH_{pp}, as shown in Fig. 2(c), extracted from Lorentzian fitting of the derivative absorption spectra, using the following equation:[28,30]

$$\Delta H_{pp} = \Delta H_0 + \frac{2}{\sqrt{3}}\frac{\alpha}{\gamma}2\pi f, \tag{2}$$

where ΔH_0 is the frequency-independent contribution arising from magnetic inhomogeneities in the LSMO thin films, and α is the intrinsic damping parameter. The damping of $\alpha \sim 1 \times 10^{-3}$ is estimated by linear fitting of the experimental data as shown in Fig. 2(c), which is slightly larger than values reported in the previous literature with different sample quality.[18] This value is comparable to reports on certain ferromagnetic metals and alloys.[31–33]

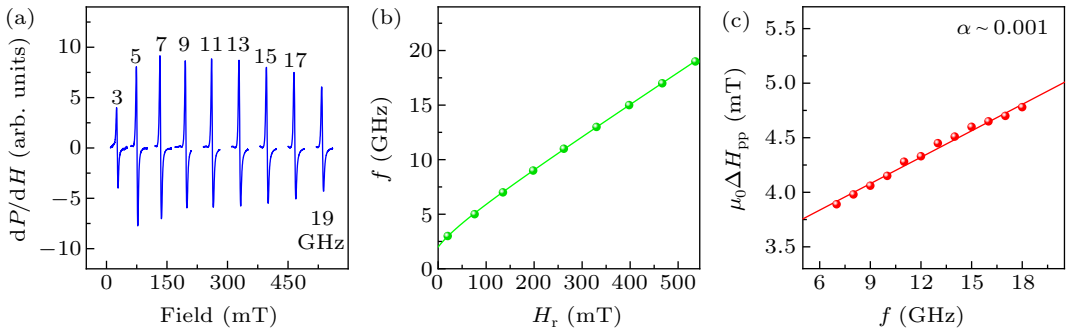


Fig. 2. Ferromagnetic resonance and magnetic damping. (a) Derivative of the absorbed power spectra of sample A measured at room temperature with fixed excitation frequencies from 3 GHz to 19 GHz. The in-plane external magnetic field is along the [010] orientation. (b) Resonance frequency f as a function of the resonance field H_r with a fitting curve consistent with Kittel's law. (c) Resonance linewidth $\mu_0\Delta H_{pp}$ as a function of resonance frequency f. The extracted magnetic damping constant α is approximately 0.001.

4. Anisotropic magnetic damping

The angle-dependent ferromagnetic resonance spectra of sample A are shown in Fig. 3. The measurements were performed at a fixed frequency of 11 GHz, with the external magnetic field rotated between the $[010]_{pc}$ and $[100]_{pc}$ orientations of the LSMO thin film. As illustrated in Fig. 3(a), the resonance peak shifts toward higher magnetic fields as the angle increases from $[010]_{pc}$ to $[100]_{pc}$, consistent with the expected in-plane magnetic anisotropy.[16] The ferromagnetic resonance spectra at different angles are fitted using Eq. (2). The anisotropy fields along the [010], [110], and [100] orientations are 3 mT, 14 mT, and 30 mT, respectively, as shown in Fig. 3(b). The angular dependence of the resonance field in Fig. 3(c) exhibits two-fold symmetric anisotropy, further confirming the magnetic anisotropy of the LSMO thin film.

It is also observed in Fig. 3(a) that the resonance linewidth of LSMO thin films exhibits significant angular dependence on the applied in-plane magnetic field. The linewidth reaches a maximum of approximately 8 mT at 0° ($[010]_{pc}$) and 90° ($[100]_{pc}$), an intermediate value of ~ 6 mT at 15° and 60°, and a minimum of ~ 4 mT at 45° ($[110]_{pc}$). Furthermore, the anisotropy of the magnetic damping is demonstrated in Fig. 3(d), exhibiting a fourfold symmetry with the minimum damping value observed along the $[110]_{pc}$ orientation. This orientation corresponds to neither an in-plane easy axis nor a hard axis, which is consistent with reported anisotropic spin-wave propagation. The damping constant shows a maximum-to-minimum ratio of ~ 150% for the 120 nm-thick film. This value is lower than the reported ratio of 200% for spin-wave lifetimes in 20 nm-thick LSMO/NGO films,[16] which is attributed to strain relaxation effects in thicker films.[11] The anisotropy of magnetic damping is influenced by multiple factors, including crystalline symmetry, orientation-dependent spin–orbit coupling (SOC), orbital degrees of freedom, and scattering effects induced by interfacial or bulk defects.[34–37] For instance, the giant damp-

ing anisotropy (400%–1400%) observed in CoFe and CoFeAl arises from variations in SOC strength across distinct magnetization orientations, corroborated by anisotropic magnetoresistance (AMR) measurements that highlight the strong correlation between SOC and damping.[34,35] In contrast, CoFeB films exhibit weak AMR–damping correlation ($\sim$ 80%), indicating additional contributions from local lattice distortions or impurity effects.[36] Notably, in Cr/Fe bilayers, a fourfold symmetric damping anisotropy of 400% persists despite negligible magnetocrystalline anisotropy, with no clear AMR–damping relationship.[37] This phenomenon cannot be fully explained by conventional SOC mechanisms or spin-pumping effects. Instead, it has been proposed that orbital Hall effects or orbital textures in the Cr layer, governed by crystallographic orientation, may dominate angular momentum dissipation. The fourfold symmetry of magnetic damping is also observed in epitaxial CoFe films, but the smallest damping is along the in-plane easy axis, which is attributed to angle-dependent spin–orbit coupling rather than two-magnon–scattering processes.[38] Therefore, the origin of anisotropic magnetic damping in LSMO thin films requires further research to be clarified.

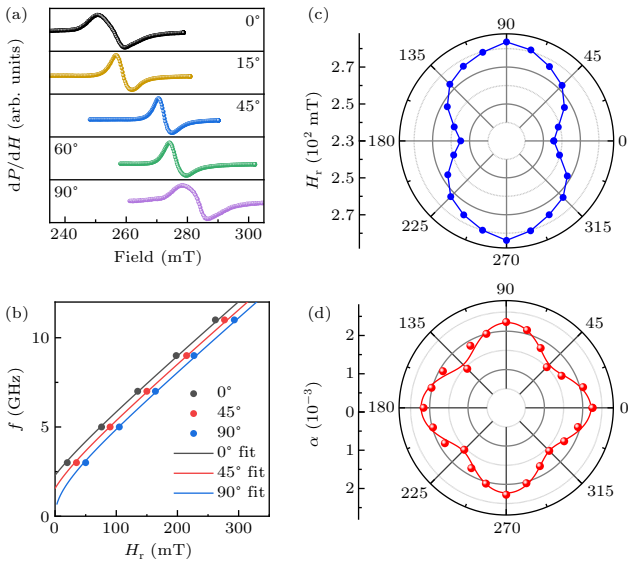


Fig. 3. Anisotropic resonance field and magnetic damping. (a) Derivative of absorbed power spectra of sample A measured at different angles. The fixed frequency is 11 GHz. The 0° (90°) angle corresponds to the external magnetic field along the [010] ([100]) orientation. (b) Resonance frequency f as a function of the resonance field H_r with a fitting curve consistent with Kittel's law at various angles. (c) Angle dependence of the resonance field H_r for sample A at 11 GHz. (d) Angle dependence of the magnetic damping α for sample A, with fitted curves exhibiting a fourfold symmetry.

5. Temperature-dependent damping

The temperature dependence of the FMR linewidth of sample A is presented in Fig. 4. The microwave absorption spectra were measured at various temperatures from 300 K to 5 K with a fixed frequency of 11 GHz, while all temperature-dependent measurements maintained an external magnetic field aligned along the $[010]_{pc}$ orientation of the LSMO thin films. Experimental measurements reveal a progressive broadening of the FMR linewidth in LSMO thin films as the temperature decreases from room temperature to cryogenic conditions, with the resonance linewidth ΔH_{pp} estimated as 5 mT at 300 K, 10 mT at 150 K, and 20 mT at 5 K, as shown in Fig. 4(a). As the temperature decreases, the resonance absorption peak shifts toward higher magnetic fields, which can be attributed to changes in the saturation magnetization and magnetocrystalline anisotropy energy.[1]

The epitaxial LSMO thin films (samples A, B, and C) were grown by slightly varying the laser energy density (0.64–0.65 J/cm^2) while maintaining other growth conditions, with samples A and B prepared at higher energy density and sample C prepared at lower energy density. Distinct surface morphologies are revealed by atomic force microscopy (AFM) characterization, as shown in Fig. 4(b). Samples A and B exhibit similar granular topography with surface roughness values of $Ra \sim 0.974$ and ~ 0.890 nm, respectively. In contrast, sample C exhibits superior quality, characterized by atomic-scale terraces, with a remarkably low roughness of $Ra\sim$ 0.087 nm, which is approximately an order of magnitude smoother than both A and B. The magnetic damping constant α of samples A, B, and C was extracted by fitting the resonance linewidth ΔH_{pp} and resonance frequency f under different temperatures, as shown in Fig. 4(c). All samples exhibit a non-monotonic damping curve, decreasing first and then increasing with decreasing temperature. A similar non-monotonic trend has also been observed in other LSMO films or heterostructures. In these reports, the temperature dependence of magnetic damping is considered to arise from contributions from spin pumping as well as resistivity-like (interband scattering) and conductivity-like (intraband scattering) mechanisms.[39,40] By contrast, the increased low-temperature magnetic damping in ferrimagnetic insulator YIG is explained by the impurity relaxation mechanism.[41]

Interestingly, although the damping values of the three samples at room temperature are relatively close, they diverge significantly at low temperatures. The magnetic damping at 5 K of samples A, B, and C is 5.7×10^{-3}, 7.4×10^{-3}, and 2.5×10^{-3}, respectively. The resonance linewidth of sample C at 5 K under 11 GHz is about 6 mT, which is significantly narrower than the 20 mT observed for sample A, as shown in Fig. 4(d). The half-metallic nature of LSMO/NGO thin films is confirmed by temperature-dependent resistivity, as shown in Fig. 4(e). The resistivity of sample C is 0.64 mΩ·cm at 300 K and 0.04 mΩ·cm at 4 K. The temperature dependence of magnetic damping in LSMO thin films is described by two terms, a resistivity-like part and a conductivity-like part, and their contributions are phenomenologically analyzed by the following

model:

$$\alpha_{\text{sum}} = \alpha_\rho \frac{\rho(T)}{\rho(300\ \text{K})} + \alpha_\sigma \frac{\sigma(T)}{\sigma(300\ \text{K})}, \tag{3}$$

where α_ρ and α_σ represent the interband and intraband scattering parameters. $\rho(T)$ and $\sigma(T)$ are the temperature-dependent resistivity and conductivity of LSMO films. The fitting result of sample C is shown in Fig. 4(f). The parameter α_ρ for resistivity-like damping is ~ 0.0018, and the parameter α_σ for conductivity-like damping is ~ 0.00013. For all samples, the suppression of magnetic damping with decreasing temperature is mainly attributed to the resistivity-like part, whereas the re-emergence below 150 K is primarily due to the conductivity-like part. The resistivity-like contribution to damping in all samples shows a similar trend, but the conductivity-like contribution exhibits a pronounced difference. As clearly seen in Figs. 4(a)–4(d), sample C with superior epitaxial quality demonstrates markedly reduced magnetic damping compared to samples A and B at low temperature. The improved epitaxial quality has significantly suppressed the contribution from the conductivity-like part associated with intraband scattering.

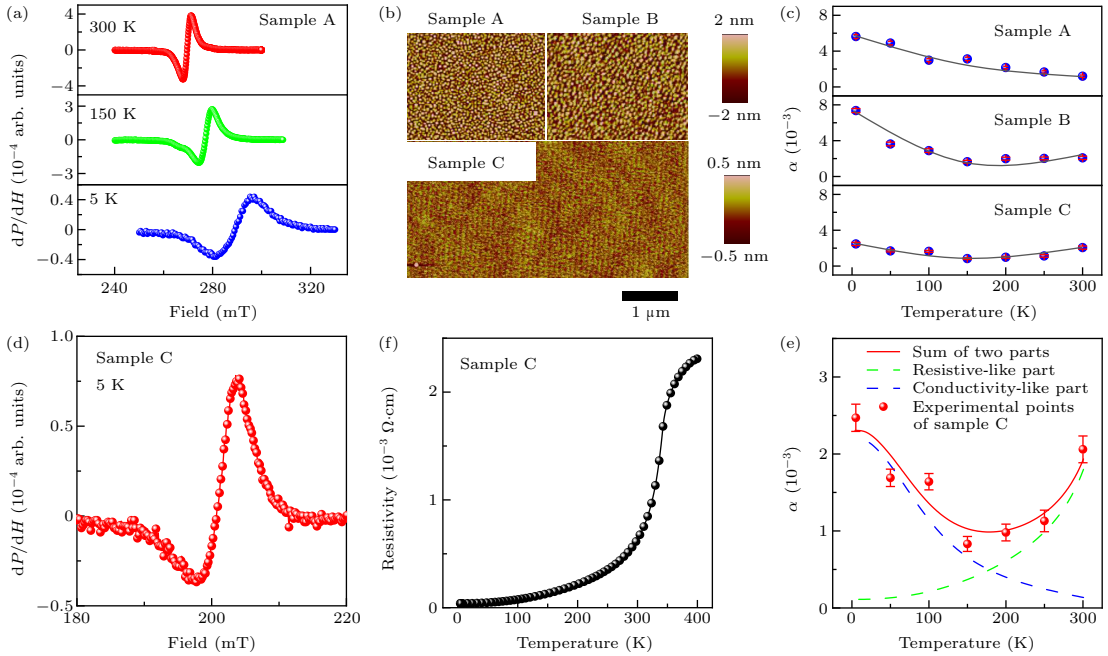


Fig. 4. Temperature-dependent magnetic damping. (a) Derivative of absorbed power spectra for sample A measured at 11 GHz under different temperatures: 300 K, 150 K, and 5 K. (b) Granular topography surfaces of samples A and B, and atomic-scale terraces of sample C. The scale bar is 1 μm. (c) Temperature-dependent magnetic damping α of samples A, B, and C from 300 K to 5 K. Grey curves are included for visual guidance. (d) Derivative of absorbed power spectra for sample C measured at 5 K under 11 GHz. (e) Resistivity as a function of temperature for sample C. (f) Analysis of the contributions from resistivity-like and conductivity-like components for the high-quality sample C.

6. Conclusion and perspectives

In summary, single-crystal epitaxial LSMO films with a thickness of 120 nm were successfully grown on NGO (110) substrates. The epitaxial quality and crystal structure were confirmed through surface topography and x-ray diffraction measurements. A fourfold symmetry of anisotropic magnetic damping was identified in the LSMO/NGO films, with a maximum-to-minimum ratio of approximately 150%. The half-metallic nature of LSMO films gives rise to a non-monotonic temperature dependence of magnetic damping. Importantly, we demonstrated that improving film quality effectively suppresses low-temperature magnetic damping by reducing intraband scattering. The highest-quality sample achieved a damping value of $\sim 2.5 \times 10^{-3}$ at 5 K.

These findings highlight an effective approach for tailoring cryogenic magnetic damping, paving the way for the exploration of quantum magnonic phenomena in manganites at low temperatures and expanding their potential applications in magnonic devices based on ferromagnet–superconductor heterostructures.

Acknowledgments

This work was supported by the National Key Research and Development Program of China (Grant Nos. 2023YFA1406500, J.Z.; 2021YFA0718700, J.Z.), the National Natural Science Foundation of China (Grant Nos. T2350005, J.Z.; 12404119, Y.Z.; 52225205, J.Z.), the Beijing Natural Science Foundation (Grant No. Z240008, J.Z.), and the Fundamental Research Funds for the Central Universities (Y.Z. and J.Z.). The authors gratefully acknowledge the 1W1A-XAFS Beamline of the Beijing Synchrotron Radiation Facility (https://cstr.cn/31109.02.BSRF.1W1A) for

providing technical support and assistance in XRD data collection.

References

[1] Kuanr B K, Veerakumar V, Kuanr A V, Camley R E and Celinski Z 2009 *IEEE Trans. Magn.* **45** 4015

[2] Lenk B, Ulrichs H, Garbs F and Münzenberg M 2011 *Phys. Rep.* **507** 107

[3] Flebus B, Grundler D, Rana B, *et al.* 2024 *J. Phys. Condens. Matter* **36** 363501

[4] Zhang X, Wang Y, Chang Y, Wang H, Rong J and Yun G 2024 *Chin. Phys. B* **33** 097601

[5] Lim Z S, Jani H, Venkatesan T and Ariando A 2021 *MRS Bull.* **46** 1053

[6] Zhang Y, Chen J, Zhang J and Yu H 2022 *Appl. Phys. Rev.* **9** 041312

[7] Jin S, Tiefel T H, McCormack M, Fastnacht R A, Ramesh R and Chen L H 1994 *Science* **264** 413

[8] Liao Z, Huijben M, Zhong Z, Gauquelin N, Macke S, Green R J, Van Aert S, Verbeeck J, Van Tendeloo G, Held K, Sawatzky G A, Koster G and Rijnders G 2016 *Nat. Mater.* **15** 425

[9] Urushibara A, Moritomo Y, Arima T, Asamitsu A, Kido G and Tokura Y 1995 *Phys. Rev. B* **51** 14103

[10] Yu X, Tokunaga Y, Taguchi Y and Tokura Y 2017 *Adv. Mater.* **29** 1603958

[11] Zhang Y, Liu J, Dong Y, Wu S, Zhang J, Wang J, Lu J, Rückriegel A, Wang H, Duine R, Yu H, Luo Z, Shen K and Zhang J 2021 *Phys. Rev. Lett.* **127** 117204

[12] Park J H, Vescovo E, Kim H J, Kwon C, Ramesh R and Venkatesan T 1998 *Nature* **392** 794

[13] Bowen M, Bibes M, Barthélémy A, Contour J P, Anane A, Lemaître Y and Fert A 2003 *Appl. Phys. Lett.* **82** 233

[14] Wahlström E, Macià F, Boschker J E, Monsen Å, Nordblad P, Mathieu R, Kent A D and Tybell T 2017 *New J. Phys.* **19** 063002

[15] Liu C, Wu S, Zhang J, Chen J, Ding J, Ma J, Zhang Y, Sun Y, Tu S, Wang H, Liu P, Li C, Jiang Y, Gao P, Yu D, Xiao J, Duine R, Wu M, Nan C W, Zhang J and Yu H 2019 *Nat. Nanotechnol.* **14** 691

[16] Wang H, Yang Y, Madami M, Wang Y, Du M, Chen J, Zhang Y, Sheng L, Zhang J, Wen C, Zhang Y, Hao S, Yu G, Han X, Gubbiotti G, Shen K, Zhang J and Yu H 2022 *Appl. Phys. Lett.* **120** 192402

[17] Zhang Y, Sheng L, Chen J, Wang J, Zhu Z, Yuan R, Lu J, Wang H, Hao S, Chen P, Yu G, Han X and Yu H 2023 *Chin. Phys. B* **32** 107505

[18] Zhang Y, Qiu L, Chen J, Wu S, Wang H, Malik I A, Cai M, Wu M, Gao P, Hua C, Yu W, Xiao J, Jiang Y, Yu H, Shen K and Zhang J 2025 *Nat. Mater.* **24** 69

[19] Zhang J, Chen M, Chen J, Yamamoto K, Wang H, Hamdi M, Sun Y, Wagner K, He W, Zhang Y, Ma J, Gao P, Han X, Yu D, Maletinsky P, Ansermet J P, Maekawa S, Grundler D, Nan C W and Yu H 2021 *Nat. Commun.* **12** 7258

[20] Wang H, Yang Y, Chen J, Wang J, Jia H, Chen P, Zhang Y, Wan C, Liu S, Yu D, Han X, Ansermet J P, Zhang J and Yu H 2023 *Phys. Rev. B* **108** 144425

[21] Chen J, Yamamoto K, Zhang J, Ma J, Wang H, Sun Y, Chen M, Ma J, Liu S, Gao P, Yu D, Ansermet J P, Nan C W, Maekawa S and Yu H 2023 *Phys. Rev. Appl.* **19** 024046

[22] Lee H K, Barsukov I, Swartz A G, Kim B, Yang L, Hwang H Y and Krivorotov I N 2016 *AIP Adv.* **6** 055212

[23] Luo G Y, Lin J G, Chiang W C and Chang C R 2017 *Sci. Rep.* **7** 6612

[24] Wahler M, Homonnay N, Richter T, Müller A, Eisenschmidt C, Fuhrmann B and Schmidt G 2016 *Sci. Rep.* **6** 28727

[25] Sanchez-Manzano D, Mesoraca S, Cuellar F A, *et al.* 2022 *Nat. Mater.* **21** 188

[26] Yuan H Y, Cao Y, Kamra A, Duine R A and Yan P 2022 *Phys. Rep.* **965** 1

[27] Boschker H, Mathews M, Houwman E P, Nishikawa H, Vailionis A, Koster G, Rijnders G and Blank D H A 2009 *Phys. Rev. B* **79** 214425

[28] Qin Q, He S, Song W, Yang P, Wu Q, Feng Y P and Chen J 2017 *Appl. Phys. Lett.* **110** 112401

[29] Rezende S M 2020 *Fundamentals of Magnonics* (Springer, Cambridge) p. 1

[30] Khodadadi B, Rai A, Sapkota A, Srivastava A, Nepal B, Lim Y, Smith D A, Mewes C, Budhathoki S, Hauser A J, Gao M, Li J F, Viehland D D, Jiang Z, Heremans J J, Balachandran P V, Mewes T and Emori S 2020 *Phys. Rev. Lett.* **124** 157201

[31] Conca A, Niesen A, Reiss G and Hillebrands B 2019 *AIP Adv.* **9** 085205

[32] Chen J R, Gong Y T, Lu X Y, Zhang C Y, Hu Y, Wang M Z, Shi Z, Fu S, Cai H L, Liu R B, Yuan Y, Lu Y, Liu T Y, You B, Xu Y B and Du J 2023 *Chin. Phys. Lett.* **40** 047501

[33] Zhan J, Wang Y, Wang X, Zhang H, Zhu S, Zhang L, Tao L, Sui Y, He W, Wan C, Han X, Belotelov V I and Song B 2024 *Chin. Phys. B* **33** 107505

[34] Li Y, Zeng F, Zhang S S L, Shin H, Saglam H, Karakas V, Ozatay O, Pearson J E, Heinonen O G, Wu Y, Hoffmann A and Zhang W 2019 *Phys. Rev. Lett.* **122** 117203

[35] Wang R, Wang W, Li Z, Gao Q, Wang J, Xu Y, Yan P, Zhang X, Zhang Y, Xu Y, Liu R and He L 2023 *Adv. Electron. Mater.* **9** 2300049

[36] Xu H, Chen H, Zeng F, Xu J, Shen X and Wu Y 2023 *Phys. Rev. Appl.* **19** 014056

[37] Nguyen T H T, Park J, Ha J H, Lee S, Nguyen V Q, Lee N J, Park B G, Cho S, Hong J I and Kim S 2024 *Phys. Rev. Mater.* **8** L041401

[38] Xia H, Zhao Z R, Zeng F L, Zhao H C, Shi J Y, Zheng Z, Shen X, He J, Ni G, Wu Y Z, Chen L Y and Zhao H B 2021 *Phys. Rev. B* **104** 024404

[39] Wang Y, Fan X, Feng X, Gao X, Ke Y, Yao J, Guo M, Wang T, Shen L, Liu M, Xue D and Fan X 2023 *Appl. Phys. Lett.* **123** 112403

[40] Haspot V, Noël P, Attané J P, Vila L, Bibes M, Anane A and Barthélémy A 2022 *Phys. Rev. Mater.* **6** 024030

[41] Jermain C L, Aradhya S V, Reynolds N D, Buhrman R A, Brangham J T, Page M R, Hammel P C, Yang F Y and Ralph D C 2017 *Phys. Rev. B* **95** 174411